The Nonforward QCD Ladder Diagrams

J. Bartels and M. Loewe[1]

II. Institut für Theoretische Physik der Universität, D-2000 Hamburg, Federal Republic of Germany

Abstract. We extend the standard analysis of the QCD planar ladder diagrams to the nonforward direction. Results are used for calculating exclusive and semiinclusive cross sections of diffractive photoproduction in the small-x region of ep-collisions. As an example we estimate the event rate for diffractive photoproduction of the neutral vector boson at Hera energies.

I. Introduction

During the last few years perturbative calculations within QCD have been applied to a large variety of hard scattering processes [1–6]. In most of these calculations evolution equations of quarks and gluons play a central rôle. Diagrammatically they corresponds (in a special gauge) to a certain class of Feynman diagrams: planar ladder diagrams, evaluated in the forward direction with their rungs taken on the mass shell (Fig. 1).

In this paper we try to extend the use of perturbation theory to cases where the same QCD ladder appears, but not necessarily in the forward direction, and the full amplitude rather than its energy discontinuity. The purpose of this extension is twofold. The original motivation comes from the observation that perturbative QCD (say, in deep inelastic ep-scattering) breaks down if the Bjorken scaling variable x becomes small (Regge-region). It is believed that then unitarity corrections become important, i.e. Feynman diagrams with more than two gluons in the exchange channel [7, 8]. A simple diagram of this type is shown in Fig 2: since the momentum transfer along the QCD-ladders has to be integrated over, this immediately leads to a study of the nonforward QCD ladder in the small-x region. Once the behavior of these ladder diagrams is

understood, one can use them – before attaching the difficult question of the Regge limit in QCD – to compute certain exclusive or inclusive processes which so far have not yet been considered in the framework of perturbative QCD. Two obvious examples are shown in Figs. 3 and 4: exclusive or (semi-) inclusive electroproduction in the small-x region of γ, neutral current, near flavor states etc. As an example which may be of practical interest for future ep-colliders (e.g. Hera) we will use our formalism to estimate the event rate for diffractive Z^0-production.
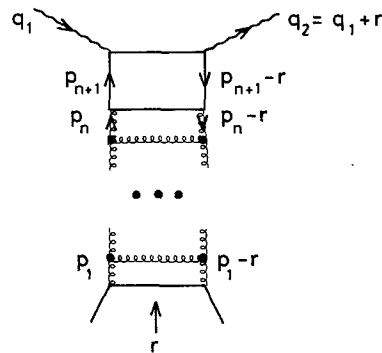
Fig. 1. The planar QCD ladder. In the small-x region the leading contributions come from gluon only. In the standard case the momentum transfer $r_\mu = 0$, and the rungs are taken to be on-shell
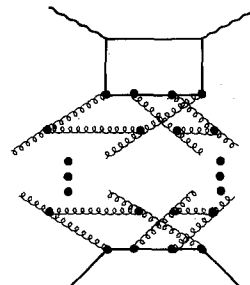
Fig. 2. Example of a QCD diagram which is expected to be important in the limit $x \to 0$

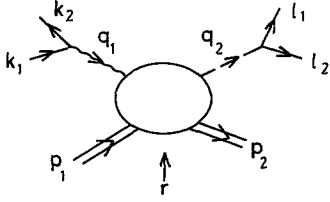1 On leave from Universidad Católica de Chile, Santiago, Chile

Fig. 3. Example of a reaction which can be described in terms of the nonforward QCD-ladder: electroproduction of the neutral current in ep-collisions
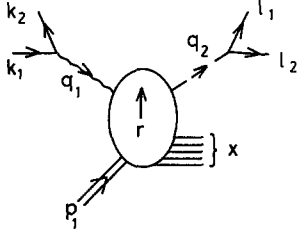

Fig. 4. Generalization of Fig. 3 to inclusive final states

Starting point for such applications is a study of the nonforward QCD ladder which will be carried out in this paper. We will start with the usual diagrammatic analysis of the QCD ladders, as they appear, for example, in ep-deep inelastic scattering [2, 3] and generalize to the case where the momentum transfer r_μ is nonzero (Fig. 1) and the rungs are not constrained to be on mass shell. We stay in the usual Bjorken limit ($Q_1^2 \to \infty$, x fixed), but we restrict ourselves to the small x-region where the gluon ladders dominate over the

quark ladders $\left(\text{but still } \frac{\alpha_s}{4\pi} \ln \frac{1}{x} \lesssim 1 \text{ such that per-}\right.$

turbative QCD is applicable$\Big)$. We believe that the use of perturbation theory can be justified within Mueller's [9] formalism of cut-vertices, but in this paper we make not attempt in this direction.

The main result of this part of our study is the behaviour of the nonforward ladder as a function of r_μ. For a purely transverse r_μ we find that a large $r_\perp^2$ prevents the formation of powers of $\ln\ln Q^2$. We thus must require that $r_\perp^2 \ll Q^2$. Moreover, if $r_\perp^2 > \mu^2$ (= typical virtuality of a valence quark inside a hadron), the integration over internal transverse momenta lies in the range $r_\perp^2 < K_\perp^2 < Q^2$ rather than $\mu^2 < K_\perp^2 < Q^2$. If r_μ is longitudinal, the usual enhancement in the small-x region persists only if the longitudinal component of r_μ is small, too. It can, however, be large enough to allow for a timelike outgoing momentum q_2.

As an immediate application of this analysis one can calculate cross sections for processes which have not yet been considered in the framework of perturbative QCD. Two obvious examples are shown in Figs. 3 and 4:

diffractive exclusive or inclusive photoproduction (in Figs. 3 and 4 we illustrate the production of the neutral current). For the inclusive reaction we derive a formalism which is quite similar to the triple-Regge formula in old hadron physics. As an example, we then calculate the cross sections for both exclusive and inclusive Z^0-production, using the data of the projected Hera-machine. As expected, these cross sections are small (the inclusive cross section gains a factor < 10 compared to the exclusive one), but still large enough to attract interest for future ep machines. The other purpose of studying the nonforward QCD-ladder, namely the $x \to 0$ limit of the deep-inelastic structure function, will be taken up in a future paper.

The outline of this paper is the following. We first study the QCD gluon ladder for $r_\mu \neq 0$. We then (Sect. III) derive a formula for semiinclusive diffraction scattering at small x. In Sect. IV we apply this to the production of the neutral vector boson, using HERA data. In the final section we conclude with a brief summary and outlook.

II. The Nonforward Ladder at Small x-Values

Our method of analysing this set of Feynman diagrams (Fig. 1) will be the following. We start from the usual diagrammatic analysis of the structure function (see, for example, [3]) which deals with the energy discontinuity of the forward ladders, and then remove both the discontinuity constraint and the condition $r_\mu = 0$. The latter part will be done in two steps: we first allow only for a transverse component $r_\perp$, then for a longitudinal component of r_μ. The results are easily summarized:

(i) The full amplitude differs from its energy discontinuity by a factor $\ln^1/x$ (and a factor 2 if we include the twisted ladder graphs). This is very similar to the Regge analysis of old φ^3-ladders: since we are working in the small x region, this analogy is easily understood;

(ii) a large transverse component $r_\perp$ prevents the formation of powers of $\ln Q_1^2$ (or, if the running coupling constant is included, powers of $\ln\ln Q_1^2$). Since the increase of the structure function at small x depends upon these powers of $\ln Q_1^2$, we conclude that only in the region $r_\perp^2 \ll Q_1^2$ we retain the maximal small-x-enhancement of the QCD-ladders;

(iii) if r_μ has a longitudinal component, the ladder diagrams depend upon two scaling variables. One belongs to the incoming (spacelike) momentum q_1, the ohter to the outgoing momentum q_2 (which can also be timelike). We find that in the small-x region the amplitude becomes large only if the longitudinal component of r_μ is sufficiently small. Moreover, it is the larger of the two-scaling variables which determines the growth.
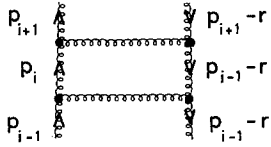
Fig. 5. A cell of the ladder diagrams of Fig. 1

Fig. 6. A single rung of Fig. 1. The symbol λ stands for gluon helicities

In the remainder of this section we briefly derive these results. We use the same techniques as in [3]. Each four momentum k_μ will be expressed in terms of Sudakov variables:

$$p_i = \alpha_i q' + \beta_i p' + p_{i\perp}, \tag{2.1}$$

where

$$q' = q_1 + xp \tag{2.2}$$

$$p' = p - \frac{\mu^2}{2v} q_1$$

are light-like reference vectors in the $(0,3)$-plane, p_μ and $q_{1\mu}$ the momenta of incoming parton and photon, respectively, and μ^2 corresponds to the initial virtuality of the incoming parton. The variables v and x are defined as usually:

$$v = pq_1 \approx p'q', \qquad x = -\frac{q_1^2}{2v} = \frac{Q_1^2}{2v}. \tag{2.3}$$

From the standard analysis we know that the dominant contribution to the structure function comes from that region of phase space where both the longitudinal and transverse components are ordered (see Fig. 1 for notation)

$$x < \beta_{n+1} < \ldots < \beta_1 < 1, \tag{2.4}$$

$$\mu^2 \ll p_{1\perp}^2 \ll \ldots \ll p_{n+1\perp}^2 \ll Q_1^2. \tag{2.5}$$

In the limit $x \to 0$ the ordering of (2.4) becomes strong.

Let us first consider the effect of removing the discontinuity constraint. In the standard case we have for each rung a factor $2\pi\delta((p_{i-1}p_i)^2)$ which can be used to do the α_i-integration

$$\alpha_i = \frac{(p_i - p_{i-1})_\perp^2}{2v(\beta_i - \beta_{i-1})^2} + \alpha_{i-1} \approx \frac{-p_{i_\perp}^2}{2v\beta_{i-1}} \tag{2.6}$$

[where we used the ordering conditions (2.4) and (2.5)]. In our case there is no such δ-function, but it is easily seen that for each cell (Fig. 5) the α_i-pole coming from the propagator of the lower rung lies in the upper half plane, whereas the α_i-poles of the other propagators lie in the lower half plane. It is therefore convenient to close the α_i-contour in the upper half plane which then has the same effect as a δ-function for each rung. The same argument goes through for each rung except for the one
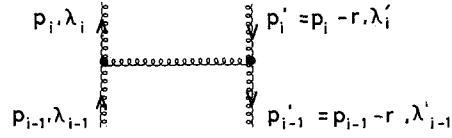
at the top of Fig. 1. Normally the δ-function for this rung leads to the condition $\beta_{n+1} = x$. Now we have for the β_{n+1}-integral a propagator instead of the δ-function:

$$\int_x^{\beta_n} d\beta_{n+1} \frac{1}{2v(\beta_{n+1} - x) - p_{n+1\perp}^2 + i\varepsilon}. \tag{2.7}$$

In the limit $v \to \infty$, the dominant contribution comes from the region $\beta_{n+1} \approx x$ and leads to the behavior $(x \to 0)$:

$$\frac{1}{2v} \ln \frac{2v}{Q_1^2} = \frac{1}{2v} \ln \frac{1}{x}. \tag{2.8}$$

Apart from the factor $\ln 1/x$, this is the same as in the case of the discontinuity. If we add to Fig. 1 its twisted analogue, we obtain an additional factor 2.

We now allow for $r_\mu \neq 0$; first we only take $r_\perp \neq 0$ and keep the other components at zero. Let us consider one rung of the ladder (Fig. 6) and compute the analogue of the Altarelli-Parisi-kernel. In the axial gauge the gluon propagator is:

$$\frac{\delta_{ab}}{k^2 + i\varepsilon} \sum_{\lambda=1,2} \varepsilon^\mu(k,\lambda) \varepsilon^\nu(k,\lambda). \tag{2.9}$$

Here $\varepsilon^\mu(k,\lambda)$ $(\lambda = 1,2)$ are the polarization vectors belonging to four momentum k_μ:

$$k_\mu = \alpha q'_\mu + \beta p'_\mu + k_{\mu\perp}$$

$$\varepsilon_\mu(k,1) = \left(0, \cos\varphi, \sin\varphi, -\frac{|k_\perp|}{\beta|\mathbf{p}|}\right) \tag{2.10}$$

$$\varepsilon_\mu(k,2) = (0, -\sin\varphi, \cos\varphi, 0)$$

(φ is the angle of the transverse component k). Using the ordering conditions (2.4) and (2.5) and keeping only that piece which is most singular in the limit $\beta_{i-1} \gg \beta_i \to 0$, we find for the numerator of the rung:

$$g^2 4N \frac{(\beta_{i-1} - \beta_i)^2}{\beta_i^2} |p_{i\perp}| |(p_i - r)_\perp| \delta_{\lambda_i 1} \delta_{\lambda'_i 1}$$

$$\cdot \begin{pmatrix} \cos(\varphi_{i-1} - \varphi'_{i-1}) & \sin(\varphi_{i-1} - \varphi'_{i-1}) \\ -\sin(\varphi_{i-1} - \varphi'_{i-1}) & \cos(\varphi_{i-1} - \varphi'_{i-1}) \end{pmatrix}_{\lambda_{i-1}\lambda'_{i-1}}. \tag{2.11}$$

When iterating such rungs, only the $(1,1)$-element of the matrix in (2.11) will contribute; we then rearrange the

$\cos(\varphi - \varphi')$ factors such that the factor $\cos(\varphi_{i-1} - \varphi'_{i-1})$ in (2.11) goes into the next-lower rung, whereas (2.11) receives a similar factor from the rung above. This replaces (2.11) by:

$$g^2 4N \frac{(\beta_{i-1} - \beta_i)^2}{\beta_i^2} |p_{i\perp}||(p_i - r)_\perp| \cos(\varphi_i - \varphi'_i)$$

$$= g^2 2N \frac{(\beta_{i-1} - \beta_i)^2}{\beta_i^2} (p_{i\perp}^2 + (p_i - r)_\perp^2 - r_\perp^2). \tag{2.12}$$

Together with the propagators of the lines p_i and $p_i - r$ and color and phase space factors we find for the i-th cell:

$$4N \frac{\alpha_{\text{bare}}}{4\pi} \int \frac{d\beta_i}{\beta_i} \int \frac{d^2 p_{i\perp}}{2\pi}$$

$$\cdot \frac{\beta_{i-1} - \beta_i}{\beta_i} \left(\frac{1}{(p_i - r)_\perp^2} + \frac{1}{p_{i\perp}^2} - \frac{r_\perp^2}{(p_i - r)_\perp^2 p_{i\perp}^2} \right). \tag{2.13}$$

In deriving this result we have used the ordering condition (2.5) for both sides of the ladders, i.e. we have assumed that

$$|p_{i-1\perp}^2| \ll |p_{i\perp}^2|, \qquad |(p_{i-1} - r)_\perp^2| \ll |(p_i - r)_\perp^2|. \tag{2.14}$$

In the standard derivation of the forward ladder ordering comes from the requirement that the integration over transverse momenta leads to the maximal number of powers of $\ln Q^2$. The result (2.13) shows that the $p_{i\perp}$-integration diverges only if $|p_{i\perp}| \gg |r_\perp|$ (in particular, the integrand is regular near $|p_{i\perp}| = 0$ and $p_{i\perp} = r_\perp$). This then leads us to the conclusion that we must have $r_\perp^2 \ll Q_i^2$ in order to obtain the maximal logarithmic enhancement from the transverse momentum integration*. Moreover if $r_\perp^2 > \mu^2$, the lower limit of the ordering condition (2.5) should be replaced by $r_\perp^2$. There is an important consistency check for the result (2.14). Dokshitser [11] has shown that the small x-behavior of the forward QCD ladders is consistent with the leading-lns Pomeron study of Kuraev et al. [12]. More precisely, by taking in the integral equation of [12] the limit of large transverse momentum and by replacing the bare coupling constant by the running coupling constant, one arrives at the same integral equation as in the small-x limit of the deep inelastic structure function. The same check can be made in our case. For $r_\perp \neq 0$ the kernel of the Pomeron integral equation [12] is:

$$\frac{(p_{i+1} - r)_\perp^2}{(p_i - r)_\perp^2 (p_i - p_{i+1})_\perp^2} + \frac{p_{i+1\perp}^2}{p_{i\perp}^2 (p_i - p_{i+1})_\perp^2} - \frac{r_\perp^2}{p_{i\perp}^2 (p_i - r)_\perp^2}. \tag{2.15}$$

---

* We do not consider the possibility that $r_\perp^2 > Q_i^2$: this would lead into the kinematic region where the form factor calculations [10] would apply

The ordering condition (2.14) immediately leads to (the transverse part of) (2.13).

Up to this point our ladders still contain the bare coupling constant. For the forward-case it has been shown that self energy corrections to gluon and quark propagator together with vertex corrections lead to the replacement in (2.13) (putting $r_\perp^2 = 0$):

$$\alpha_{\text{bare}} \to \alpha(p_{i\perp}^2). \tag{2.16}$$

In our case the same argument holds, at least as long as in (2.13) $|p_{i\perp}|^2 \gg |r_\perp|^2$: we then simply disregard $r_\perp^2$. At the lower end of the integration, however, $p_{i\perp}^2 \sim r_\perp^2$, and (2.16) needs to be modified. We shall assume that we have, instead of (2.16):

$$\alpha_{\text{bare}} = \frac{g_{\text{bare}}^2}{4\pi} \to \frac{g(p_{i\perp}^2)g((p_i - r)_\perp^2)}{4\pi}. \tag{2.17}$$

As a result of this, the difference between the forward ladder and the nonforward case (only $r_\perp \neq 0$) consists of the following change:

$$\xi(Q^2) = \int_{\mu^2}^{Q^2} \frac{dp_\perp^2}{p_\perp^2} \frac{\alpha_s(p_\perp^2)}{4\pi} \to \int_{r_\perp^2}^{Q^2} \frac{dp_s^2}{p_\perp^2} \frac{g(p_\perp^2)g((p - r)_\perp^2)}{(4\pi)^2}. \tag{2.18}$$

As long as $r_\perp^2 \ll Q^2$, this change will not affect the leading behavior as $Q^2 \to \infty$.

Next we allow r_μ to have a nonzero longitudinal component β_r (for simplicity, $r_\perp^2 = 0$ again). Repeating the analysis which leads to (2.13), we find, as the only change:

$$\frac{\beta_{i-1} - \beta_i}{\beta_i^2} \to \frac{\beta_{i-1} - \beta_i}{\beta_i \beta'_i}, \qquad \beta'_i = \beta_i - \beta_r. \tag{2.19}$$

As we have mentioned before (2.11), this only represents the most singular (in the limit $\beta_{i-1} \gg \beta_i \to 0$) piece of the kernel. It follows, however, from (2.19) that this singularity will be lost if $\beta_r \neq 0$ when $x \to 0$. This situation will become clearer, if we write down the full chain of β-integrals of Fig. 1:

$$\int_{=x}^{1} d\beta_n \frac{\beta_{n-1} - \beta_n}{\beta_n \beta'_n} \int_{\beta_n}^{1} d\beta_{n-1} \frac{\beta_{n-2} - \beta_{n-1}}{\beta_{n-1} \beta'_{n-1}} \cdots \int_{\beta_2}^{1} d\beta_1 \frac{1 - \beta_1}{\beta_1 \beta'_1}. \tag{2.20}$$

If β_r would be zero, i.e. all $\beta'_i = \beta_i$, this integral would diverge as $1/x(\ln 1/x)^{n-1}$ (in the limit $x \to 0$). This divergence is due to that region of phase space where

$$x \ll \beta_n \ll \cdots \ll \beta_1 \ll 1. \tag{2.21}$$

In our case, however, we want $\beta_r \neq 0$. Then such a small-x-enhancement is possible only of we require that β_r is also small, i.e.

$$\beta_r \to 0 \quad \text{together with} \quad x \to 0. \tag{2.22}$$

Let us consider two cases. If $\beta_r \ll x$, then β_r can safely be neglected everywhere in (2.20) and we still have the same behavior: $1/x(\ln 1/x)^{n-1}$. In the more interesting case, however, we want the outgoing momentum q_2 to be timelike. For this we need $\beta_r > x$, for example $\beta_r = cx$ with $c > 1$. With $\alpha_r \ll 1$ (this follows from the mass-shell conditions of the outgoing parton at the lower end of the ladder) we then have:

$$q_2^2 = 2\nu(\beta_r - x) + r_\perp^2 > 0 .\qquad (2.23)$$

So if we require $\beta_r > x$, the β_i-integrals in (2.20) cannot go down to x (otherwise $\beta_i' = \beta_i - \beta_r$ could become negative and the partons on the right hand side of the ladder would run into the opposite direction) but only down to $c'\beta_r$ ($c' > 1$). This replaces (2.20) by

$$\int\limits_{c'\beta_r}^{1} d\beta_n \frac{\beta_{n-1}-\beta_n}{\beta_n\beta_n'} \int\limits_{\beta_n}^{1} d\beta_{n-1} \frac{\beta_{n-2}-\beta_{n-1}}{\beta_{n-1}\beta_{n-1}'} \dots \int\limits_{\beta_2}^{1} d\beta_1 \frac{1-\beta_1}{\beta_1\beta_1'} \qquad (2.24)$$

and leads to $1/\beta_r(\ln^1/\beta_r)^{n-1}$ (up to constant factors). From this we conclude that it is always the larger variable of x and β_r which sets the scale in the small-x region.

In order to complete our discussion of the nonforward QCD ladder, we still have to couple a quark line to the lower end and a quark loop to the upper end of our gluon ladder. For simplicity, we shall do this only for the case $r_\perp^2 = 0$. At the lower end we make use of the strong ordering condition [(2.21) and (2.22)]: β_r can then safely be neglected. As to the summation over the quark helicities (Fig. 7), it is well known [13] that a fast quark at the quark-gluon vertex conserves helicity. As a result of this, the quark helicities are equal at both sides of the ladder, and we are back at the usual Altarelli-Parisi expression for the fermion rung. At the upper end we have for the trace:

$$\mathrm{Tr}[\not{p}(p_n - r, 1)(\not{p}_{n+1} - \not{r})\gamma_\mu(\not{p}_{n+1} + \not{q}_1)$$

$$\cdot \gamma_\nu(\not{p}_{n+1}\not{p}(p_n, 1)(\not{p}_n - \not{p}_{n+1})]$$

$$\approx 4\nu\left(-g_{\mu\nu} + \frac{p_\mu' q_\nu' + p_\nu' q_\mu'}{\nu}\right)$$

$$\cdot \left\{\beta_{n+1} - \beta_r + \beta_{n+1} + \frac{\beta_n(\beta_n - \beta_r)}{\beta_n - \beta_{n+1}}\right\} |p_{m+1\perp}^2| \qquad (2.25)$$

which is regular near $\beta_{n+1} = 0$. Because of the argument contained in (2.7), the β_{n+1}-integration effectively leads to $\beta_{n+1} = x$. Thus the fermion loop, when coupled to the gluonic ladder, will not change the small-x behavior (i.e. no additional power of $\ln 1/x$), but modifies the result (2.23) merely by a constant factor which weakly depends upon whether $\beta_r \ll x$ or $x \ll \beta_r$. To leading order, therefore, the effect of the fermion loop is the same as in the forward direction.

Fig. 7. The fermion line at the lower end of Fig. 1

We summarize the results of this section in the following expression for the gluon ladder, valid to leading order in the limit $x \to 0$, $\beta_r \to 0$:

$$F_{\mu\nu}(\bar{x}, \xi) = \left(-g_{\mu\nu} + \frac{p_\mu' q_\nu' + p_\nu' q_\mu'}{\nu}\right) \cdot 2\ln\frac{1}{\bar{x}} \cdot \frac{64 C_2 \xi^2}{3\bar{x}\sqrt{2\pi}}$$

$$\cdot \frac{\exp\sqrt{16N\xi\ln 1/\bar{x}}}{(16N\xi\ln 1/\bar{x})^{5/4}} . \qquad (2.26)$$

Here $\bar{x}$ is equal to $\max(x, \beta_r)$, and ξ is taken from (2.18), deviating from the usual ξ-variable only if $\mu^2 \ll r^2$ (but always $r_\perp^2 \ll Q_1^2$).

III. The Inclusive Cross Section

We now want to make use of the results of the previous section and calculate a few cross sections. The most straightforward applications are various diffractive photoproduction processes in the small-x region, for example production of lepton pairs, new flavor states, Z^0-production, ... One of them, the production of the Z^0-boson (Fig. 3) will be estimated in the following section. Before this we wish to generalize to another type of reactions: inclusive photoproduction. One example, which will also be considered in the next section, is again the production of Z's (Fig. 4). In this section, we develop the necessary formalism which then allows the calculation of such reactions.

The class of QCD Feynman diagrams which is relevant for such inclusive processes is shown in Fig. 8 (we always stay in the axial gauge). These diagrams consist of three parts:

a) The usual distribution function of deep inelastic ep-scattering which is responsible for the inclusive part of the final state;

b) a branching vertex whose position in $x, k_\perp^2$-space restricts the phase space of the inclusively produce hadrons, and

c) the two nonforward ladders above the branching vertex. Since (so far) we know them only on the small-x region, the upper ends of these ladders must be sufficiently "far away" in x-space from the branching vertex.

The parts *a)* and *c)* can immediately be taken from the literature [3] and the previous section, respectively, whereas the branching vertex requires some discussion.
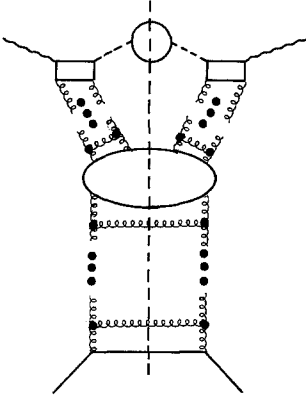
Fig. 8. The class of Feynman diagrams which describes the reaction of Fig. 4. In the small x-region only gluonic ladder diagrams contribute
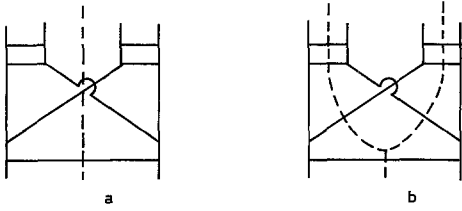
Fig. 9a and b. The nonplanar branching vertex. a shows the energy discontinuity which is relevant for the reaction Fig. 4. The energy discontinuity of **b** applies to the jetcalculus of [14]
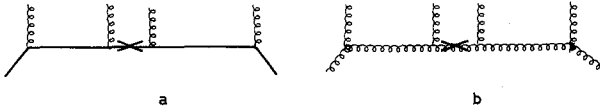
Fig. 10a and b. The planar model for the branching vertex that we use in this paper

The kinematics of our inclusive process is very close to that of the triple-Regge region in hadron-hadron scattering; there one knows that the coupling between the three ladders has to be nonplanar. This suggests that the branching vertex of our case should be nonplanar, too (Fig. 9). The calculation of this vertex, however, shows that ordering of the transverse momenta which is not present in Regge physics slightly changes the situation. First one finds that the "diffractive cut" through the vertex (as shown in Fig. 9a) does not lead to the same answer as the (so-called double multiperipheral) cut shown in Fig. 9b which is relevant for the jet calculus [14]. This is in contrast to the situation in hadronic physics, and it indicates that another feature of Regge physics, namely the cancellation of Regge cuts in planar diagrams, also does not hold because of ordering of the transverse momentum. For our present purposes (in particular for the numerical estimate in the following section) we, therefore, take a simpler model for the branching vertex: the planar graph shown in Fig. 10.

After these remarks we are ready to derive our formula for the inclusive cross section. We first study the planar vertex of Fig. 10 and find that in the limit where the longitudinal components above the vertex are much smaller than those below, it equals the square of the usual Altarelli-Parisi-kernel. In other words, we find for the numerators of Fig. 10:

numerator of Fig. 10a

$$= g_s^4 C_2^2(-p^2)(-p'^2)\frac{(1-z)^2+1}{z^2}\frac{(1-z')^2+1}{z'^2} \qquad (3.1)$$

and

numerator of Fig. 10b

$$\approx_{z,z'\to 0} g_s^4(4N)^2(-p^2)(-p'^2)\frac{(1-z)^2}{z^2}\frac{(1-z')^2}{z'^2}. \qquad (3.2)$$

Next we combine this with the other parts of Fig. 8. We find:

$$F_{\mu\nu;\mu'\nu'} = \int_{\bar{x}}^{1}\frac{dy_B}{y_B}\left\{\delta(1-y_B)F_{\mu\nu}\left(\frac{\bar{x}}{y_B},\xi\right)F_{\mu'\nu'}\left(\frac{\bar{x}}{y_B},\xi\right)\right.$$

$$+ \int_{0}^{\xi_{max}} d\xi_B\cdot\left(\frac{\partial}{\partial\xi_B}W(y,\xi_B)\right)$$

$$\left.\cdot F_{\mu\nu}\left(\frac{\bar{x}}{y_B},\xi-\xi_B\right)\cdot F_{\mu'\nu'}\left(\frac{\bar{x}}{y_B},\xi-\xi_B\right)\right\}. \qquad (3.3)$$

Here y_B, ξ_B denote longitudinal momentum and virtuality at the branching vertex. The first term in (3.3) stands for those diagrams where the upper two gluon ladders couple directly to the fermion line at the bottom. In the second part the derivative takes care of the fact that the ξ-integration in the loop underneath the branching vertex cannot be absorbed into the lower ladder: it acts both as the lower limit of the upper two ladders and as the upper limit of the lower ladder. The functions $F_{\mu\nu}$ and W are normalized such that in the small-x-region they behave as:

$$F_{\mu\nu}(z,\xi) = \left(-g_{\mu\nu}+\frac{p'_\mu q'_\nu+p'_\nu q'_\mu}{\nu}\right)$$

$$\cdot 2\ln\frac{1}{z}\int\frac{dj_1}{2\pi i}z^{-j_1}\frac{16C_2}{3}\frac{j_1-1}{4N}e^{j_1-1}^{\frac{4N\xi}{}}$$

$$\approx \left(-g_{\mu\nu}+\frac{p'_\mu q'_\nu+p'_\nu q'_\mu}{\nu}\right)$$

$$\cdot 2\ln\frac{1}{z}\frac{64C_2\xi^2\exp\sqrt{16N\xi\ln 1/z}}{(16N\xi\ln 1/z)^{5/4}} \qquad (3.4)$$

and

$$W(z,\xi) = \frac{4N}{4C_2}\int\frac{dj}{2\pi i}z^{-j}e^{j-1}^{\frac{4N\xi}{}}. \qquad (3.5)$$

If we insert the Mellintransforms (3.4) and (3.5) into (3.3), we find, for the second part, that the integration over y_B leads to the conservation law of angular momentum:

$$j = j_1 + j_2 - 1, \tag{3.6}$$

where j_1 and j_2 belong to the upper two ladders and j to the lower one. This situation is quite reminiscent of the triple-Regge analysis in hadron-hadron scattering or the jet-calculus. Before presenting our final answer we mention that the integration over ξ_B in (3.3) cannot go up to ξ. As usual, our perturbative analysis is valid only if $\ln 1/x < \ln Q^2/\Lambda^2$. We therefore keep ξ_B smaller than some $\xi_{max} < \xi$.

Putting all this together we use the saddle-point method and derive the following small-x limit for the second part of (3.3):

$$F_{\mu\nu;\mu'\nu'} \approx g^{\perp}_{\mu\nu} g^{\perp}_{\mu'\nu'} \int_0^{\xi_{max}} d\xi_B \left[2 \cdot \ln \frac{1}{\overline{x}} \cdot \frac{64 C_2 (\xi - \xi_B)^2}{3 \sqrt{2\pi\overline{x}}} \cdot \frac{\exp \sqrt{4N \ln 1/\overline{x}(\xi - \xi_B) W_B^{-1}} \cdot \exp \sqrt{4N \ln 1/\overline{x}(\xi - \xi_B) W_B}}{(16 N \ln 1/\overline{x}(\xi - \xi_B) W_B^{-1})^{5/4}} \right]$$

$$\cdot \frac{1}{\sqrt{W_B}} \cdot \frac{4N}{4C_2} \cdot \frac{1}{2} \sqrt{\frac{4N \ln 1/\overline{x}}{(\xi - \xi_B) W_B}} \exp \frac{1}{2} \sqrt{4N \xi_B^2 (\xi - \xi_B)^{-1} \ln 1/\overline{x} W_B^{-1}} \tag{3.7}$$

with

$$W_B = 1 + \frac{1}{4} \frac{\xi_B}{\xi - \xi_B}, \qquad g^{\perp}_{\mu\nu} = g_{\mu\nu} - \frac{p'_\mu q'_\nu + p'_\nu q'_\mu}{\nu}.$$

As a function of ξ_B, the integrand of (3.7) has its maximum near $\xi_B = 0$ where it becomes equal to the first term of (3.3), apart from the enhancement factor

$$\frac{4N}{4C_2} \frac{1}{2} \sqrt{\frac{4N \ln 1/\overline{x}}{\xi}}. \tag{3.8}$$

IV. Z^0-Production

In this section we investigate, as an application of our calculations, the possibility of diffractive Z^0-production in a $e - p$ collider. We first consider the exclusive process $e + p \to e + p + Z^0 \to e + p + (\mu^+ \mu^-)$ (Fig. 3a), then the semiinclusive reaction $e + p \to e + Z^0 + \text{anything} \to e + (\mu^+ \mu^+) + \text{anything}$ (Fig. 3b).

With the notation of Fig. 3a we have for the differential cross section:

$$d\sigma = \frac{1}{2} \sum_{\text{Spins}} \left| \bar{u}(k_1) e \gamma^\mu u(k_2) \frac{g_{\mu\nu}}{q_1^2} e^2 \tilde{F}^{v\varrho} \mathscr{D}^Z_{\varrho\sigma}(q_2^2) \right.$$

$$\left. \cdot \frac{1}{\sin^2 \Theta_W \cos^2 \Theta_W} \bar{v}(l_1) j^\sigma_{\text{neutral}} e u(l_1) \right|^2$$

$$\cdot (2\pi)^4 \delta^4(r + q_1 - l_1 - l_2) \frac{1}{|v_e - v_p|} \frac{1}{2E_{p_1} 2E_{k_1}}$$

$$\cdot \frac{d^3 k_2}{2E_{k_2}(2\pi)^3} \frac{d^3 r}{2E_{p_2}(2\pi)^3} \frac{d^3 l_1}{2E_{e_1}(2\pi)^3} \frac{d^3 l_2}{2E_{e_2}(2\pi)^3}. \tag{4.1}$$

In this formula we have averaged over initial and summed over final spins. $\tilde{F}_{v\varrho}$ is the structure function of (2.26), convoluted with the valence quark distribution function inside the proton:

$$\tilde{F}_{v\varrho}(\overline{x}, \xi) = \sum_{u,d} \int_{\overline{x}}^1 \frac{dz}{z} w^{u,d}(z) F_{v\varrho}\left(\frac{\overline{x}}{z}, \xi\right). \tag{4.2}$$

The coupling of the neutral current to quarks and leptons is given by [15]:

$$j^\mu_{\text{neutral}} = (\bar{e}\bar{\mu}\bar{\tau}) \left\{ -\frac{1}{2} \gamma^\mu \frac{1 - \gamma_5}{2} + \sin^2 \Theta_W \gamma^\mu \right\} \begin{pmatrix} e \\ \mu \\ \tau \end{pmatrix}$$

$$+ (\bar{u}\bar{c}\bar{t}) \left\{ \frac{1}{2} \gamma^\mu \frac{1 - \gamma_5}{2} - \frac{2}{3} \sin^2 \Theta_W \gamma^\mu \right\} \begin{pmatrix} u \\ c \\ t \end{pmatrix}$$

$$+ (\bar{d}\bar{s}\bar{b}) \left\{ -\frac{1}{2} \gamma^\mu \frac{1 - \gamma_5}{2} + \frac{1}{3} \sin^2 \Theta_W \gamma^\mu \right\} \begin{pmatrix} d \\ s \\ b \end{pmatrix}. \tag{4.3}$$

The γ_5-piece in the coupling of the neutral current to the fermion box in Fig. 3a drops out as a result of C-conjugation. Summation over the spins in (4.1) and integration over the momenta of the lepton pair leads to:

$$\sum_{\text{Spins}} e^2 \int \frac{d^4 l_1}{(2\pi)^4} \bar{v}(l_1) j^\mu_{\text{neutral}}$$

$$\cdot u(q_1 + r - l_1) \bar{u}(q_1 + r - l_1) j^\nu_{\text{neutral}} v(l_1)$$

$$\cdot (2\pi)^2 \cdot \delta^+(l_1^2 - m_\mu^2)(\slashed{l}_1 + m_\mu)$$

$$\cdot \delta^+((q_1 + r - l_1)^2 - m_\mu^2)(\slashed{q}_1 + \slashed{r} + \slashed{l}_1 + m_\mu)$$

$$\underset{q_2^2 \gg m_\mu^2}{\approx} \frac{2\alpha}{3} (-g^{\mu\nu}(q_1 + r)^2 + (q_1 + r)^\mu (q_1 + r)^\nu)$$

$$\cdot \left(\left(\frac{1}{4} - \sin^2 \Theta_W \right)^2 + \frac{1}{16} \right). \tag{4.4}$$

Finally, the Z^0-propagator is taken to be:

$$\mathscr{D}^Z_{\mu\nu}(q^2) = \frac{g_{\mu\nu} - q_\mu q_\nu / M_z^2}{q^2 - M_z^2 + i\Gamma M_z}. \tag{4.5}$$

We now insert (2.26) into (4.1) and contract all the Lorentz indices, using

$$k_{2\perp}^2 = x \frac{s_T}{2\nu}(s_T - 2\nu). \tag{4.6}$$

We use the mass-shell condition of the outgoing proton, in order to do the α_r-integration:

$$-\alpha_r = \frac{M^2 + r_\perp^2}{2v(1-\beta_r)}. \qquad (4.7)$$

This then leads to:

$$
\begin{aligned}
d\sigma = {} & \frac{32\alpha^4}{3} \frac{q_2^2}{(q_2^2 - M_z^2 + i\Gamma M_r)^2} \frac{1}{s_T Q_1^2} \\
& \cdot \frac{s_T + (s_T - 2v)^2}{(2v)^2} \frac{d^3 k_2}{2E_{k_2}(2\pi)^3} \\
& \cdot \frac{1}{(\sin\Theta_W \cos\Theta_W)^4}\left(\left(\frac{1}{4} - \sin^2\Theta_W\right)^2 + \frac{1}{16}\right) \\
& \cdot \left(\frac{3}{4} - \frac{5}{3}\sin^2\Theta_W\right)\frac{d\beta_r d^2 r_\perp}{(1-\beta_r)} \\
& \cdot \left[\sum_{n,d}\int_{\bar{x}}^1 \frac{dz}{z} w^{n,d}(z) 2\ln\frac{z}{x}\right. \\
& \left. \cdot \frac{64 C_2 \xi^2 \exp\left|\sqrt{16N\xi\ln z/\bar{x}}\right|^2}{3\sqrt{2\pi\bar{x}/z}(16N\xi\ln z/\bar{x})^{5/4}}\right]. \qquad (4.8)
\end{aligned}
$$

Before we insert numbers into this expression we have to make a few comments. From our discussion at the end of Sect. II we know that in order to make the cross section as large as possible we need:

1) the exchanged transverse momentum $r_\perp$ is as small as possible. We, therefore, evaluate our cross section at $r_\perp^2 = 0$ and keep only events with $r^2 \lesssim 10\,\text{GeV}^2$. This leads to:

$$\int d^2 r_\perp \to \pi \cdot 10 M^2 \qquad (M = \text{nucleon mass}). \qquad (4.9)$$

2) The longitudinal momenta of both the virtual photon and the neutral current are as small as possible. However, the requirement that the neutral current carries enough energy to produce a resonance of, say, 90 GeV, sets a lower limit to the longitudinal momentum of the neutral current. In the notation of Sect. II we have:

$$Q_2^2 \sim 2v(\beta_r - x). \qquad (4.10)$$

If we denote by s the energy of the hadronic part, we have for small x

$$s = (p_1 + q_1)^2 = q_1^2 + 2v = 2v(1-x) \approx 2v. \qquad (4.11)$$

From the condition that s cannot be larger than the total energy $s_T = (p_1 + k_1)^2$ we obtain:

$$s \approx 2v = \frac{Q_2^2}{\beta_r - x} \lesssim s_T$$

$$\tilde{x} = \beta_r - x \gtrsim \frac{Q_r^2}{s_T}. \qquad (4.12)$$

With the data of Hera [16]: $s_T \approx 4E_p E_e \approx 10^5\,\text{GeV}^2$ and $M_z^2 = 8000\,\text{GeV}^2$ we find:

$$\tilde{x} = \beta_r - x \gtrsim 0.08. \qquad (4.13)$$

For a numerical estimate of our cross section (4.8) we take both x and $\beta_r - x$ to be 0.1. This is also the region where our approximation of only keeping the gluonic part of the QCD ladders is valid. It is also convenient to parametrize in (4.8) the final states through $Q_2^2 = $ mass of the neutral current and the longitudinal momenta and $\beta_r - x = \tilde{x}$ rather than the momentum of the outgoing electron. The Jacobian for this transformation is:

$$\frac{d^3 k_2}{2E_{k_2}(2\pi)^3} = \frac{1}{2(2\pi)^2 s_T}\int dx\, dQ_2^2 \frac{Q_2^2}{2(\beta_r - x)^2}. \qquad (4.14)$$

Our cross section (4.8) then becomes:

$$
\begin{aligned}
\frac{d\sigma}{dx\,d\tilde{x}\,dQ_2^2} = {} & \frac{16\alpha^4}{3(2\pi)} \cdot \frac{10M^2}{s_T^2} \cdot \frac{1}{xQ_2^2(Q_2^2 - M_z^2 + i\Gamma M_z)^2} \\
& \cdot \frac{\left((\frac{1}{4} - \sin^2\Theta_W)^2 + \frac{1}{16}\right)(\frac{3}{4} - \frac{5}{3}\sin^2\Theta_W)^2}{(\sin\Theta_W \cos\Theta_W)^4} \\
& \cdot \frac{\tilde{x}}{1 - x - \tilde{x}}\left(s_T^2 + \left(s_T - \frac{Q_2^2}{\tilde{x}}\right)^2\right) \\
& \cdot \left[\sum_{u,d}\int_{\bar{x}}^1 \frac{dz}{z} w^{u,d}(z)\ln\frac{z}{\bar{x}}\right. \\
& \left. \cdot \frac{64 C_2 \xi^2 \exp\left|\sqrt{16N\xi\ln z/\bar{x}}\right|^2}{3\sqrt{2\pi\bar{x}/z}(16N\xi\ln z/\bar{x})^{5/4}}\right], \qquad (4.15)
\end{aligned}
$$

where

$$\tilde{x} = \beta_r - x,$$

$$\xi = \frac{1}{b}\ln\ln Q_1^2/\Lambda^2 = \frac{1}{b}\ln\ln\left(\frac{Q_2^2}{\Lambda^2}\cdot\frac{x}{\tilde{x}}\right),$$

$$b = 11 - \frac{2}{3}n_f,$$

$$\bar{x} = \max(x, \beta_r) = \beta_r = 0.2.$$

We finally insert numbers. Parameters of the Hera machine are [16]:

$$E_p = 820\,\text{GeV}, \qquad E_k = 30\,\text{GeV} \qquad (4.16)$$
$$\text{Luminosity} = 0.35 \times 10^{32}\,\text{s}^{-1}\,\text{cm}^{-2}.$$

For the QCD part we use [17]:

$$\Lambda = 0.1\,\text{GeV}$$
$$n_f = 6$$
$$w^u(z) = \frac{1.79}{\sqrt{z}}(1-z)^3(1+2.3z)$$
$$w^d(z) = \frac{1.10}{\sqrt{z}}(1-z)^{3.1}. \qquad (4.17)$$

The weak interaction parameters are [18]:

$$M_z = 90\,\text{GeV}, \quad \Gamma = 2.5\,\text{GeV}, \quad \sin^2\Theta_W = \tfrac{1}{4}. \quad (4.18)$$

The z-integral in (4.15) can be done approximately (in the limit of small x) and leads to an effective enhancement factor:

$$\int_{\bar{x}}^{1} \frac{dz}{z}\, w^{u,d}(z)\, \frac{64 C_2 \xi^2 \exp\sqrt{16 N \xi \ln z/\bar{x}}}{\bar{x}/z (16 N \xi \ln z/\bar{x})^{5/4} 3\sqrt{2\pi}}\, \ln z/\bar{x}$$

$$\underset{x\to 0}{\approx} C^{u,d}\, \frac{64 C_2 \xi^2 \exp\sqrt{16 N \xi \ln 1/\bar{x}}}{3\sqrt{2\pi}\,\bar{x}(16 N \xi \ln 1/\bar{x})^{5/4}}\cdot \ln 1/\bar{x}, \quad (4.19)$$

where

$$C^u \approx 2, \quad C^d \approx 1. \quad (4.20)$$

In the variables Q_2^2, x, and $\bar{x}$ we allow ranges of $500\,\text{GeV}^2$, 0.1, and 0.1, respectively. This then leads to:

$$10^{-2}\ \text{events/day}. \quad (4.21)$$

It is important to emphasize that this result takes into account only the most singular part (in the limit x, $\beta_r \to 0$) of the ladder diagrams. Nonleading pieces will still be relevant at Hera-energies, and it would therefore be of interest to extend our analysis beyond the leading approximation.

We now turn to the semiinclusive process of Fig. 3b. Our result of (3.3) allows us to restrict the inclusively produced hadrons to a kinematic region which is close to the outgoing proton. For example, we could demand that $y_B > y_{\min}$ and $k_{B\perp}^2 < k_{\perp\,\max}^2$ (i.e. $\xi_B < \xi_{\max}$): the hadrons then have momenta larger than $y_B\cdot|p_{\text{proton}}|$ and they are produced within a cone of opening Θ:

$$\tan^2\Theta = \frac{k_{\perp\,\max}^2}{(y_{\min}|p_{\text{proton}}|)^2}. \quad (4.22)$$

Such events have the advantage of being rather clean, i.e. the produced lepton pair is well separated from the produced hadrons.

However, in order to make our estimate as simple as possible, we will allow for the full region of y_B, and for $k_{B\perp}^2 < k_{\perp\,\max}^2 \approx 20\,\text{GeV}^2$. From the derivation of (3.3) we know that the main contribution will come from the region where

$$x, \bar{x} < y_B < 1. \quad (4.23)$$

So at least most of the inclusively produced hadrons will be separated from the μ-pair. The differential cross section is given by:

$$d\sigma = \frac{1}{2}\sum_{\text{Spins}} \left| \bar{u}(k_1) e\gamma^{\mu_1} u(k_2)\, \frac{g_{\mu_1 v_1}}{q_1^2} \right.$$

$$\cdot\, e^2 \mathscr{D}^z_{\varrho_1 \sigma_1}(q_2^2)\bar{v}(l_1) j^{\sigma_1}_{\text{neutral}} e u(l_2) \Big|$$

$$\cdot\, \left| \bar{u}(k_1) e\gamma^{\mu_2} u(k_2)\, \frac{g_{\mu_2 v_2}}{q_1^2} \right.$$

$$\cdot\, e^2 \mathscr{D}^z_{\varrho_2 \sigma_2}(q_2^2)\bar{v}(l_1) j^{\sigma_2}_{\text{neutral}} e u(l_2) \Big|$$

$$\cdot\, (\sin\Theta_W \cos\Theta_W)^{-4}\, \tilde{F}^{v_1 \varrho_1;\, v_2 \varrho_2}$$

$$\cdot\, (2\pi)^4 \delta^4(r + q_1 - l_1 - l_2)$$

$$\cdot\, \frac{1}{2E_{e_1} 2E_{k_1} |v_e - v_p|}\frac{d^4 r}{(2\pi)^4}\frac{d^3 k_2}{2E_{k_2}(2\pi)^3}$$

$$\cdot\, \frac{d^3 l_1}{2E_{e_1}(2\pi)^3}\frac{d^3 l_2}{2E_{e_2}(2\pi)^3}. \quad (4.24)$$

The tensor $\tilde{F}_{v_1 \varrho_1;\, v_2 \varrho_2}$ is taken from (3.3); the tilde-symbol indicates that we convoluted our result (3.3) with the valence quark distribution function. We perform the same steps as those which lead to (4.15) and use the small-x approximation (3.7). The result then is:

$$\frac{d\sigma}{dx\,d\bar{x}\,dQ_2^2} = \frac{16\alpha^4}{3(2\pi)}\frac{10 M^2}{s_T^2}\frac{1}{x Q_2^2 (Q_2^2 - M_z^2 + i\Gamma M_z)^2}$$

$$\cdot\, \frac{((\tfrac{1}{4} - \sin^2\Theta_W)^2 + \tfrac{1}{16})(\tfrac{3}{4} - \tfrac{5}{3}\sin^2\Theta_W)^2}{(\sin\Theta_W \cos\Theta_W)^4}\frac{\bar{x}}{(1 - x - \bar{x})}\left(s_T^2 + \left(s_T - \frac{Q_2^2}{\bar{x}}\right)^2\right)$$

$$\cdot\, \sum_{u,d}\int_{\bar{x}}^{1}\frac{dz}{z}\, w^{u,d}(z)\left\{\left[\ln\frac{z}{\bar{x}}\, \frac{64 C_2 \xi^2 \exp\sqrt{16 N \xi \ln z/\bar{x}}}{3\sqrt{2\pi}\,\bar{x}/z (16 N \xi \ln z/\bar{x})^{5/4}}\right]^2\right.$$

$$+ \int_{0}^{\xi_{\max}} d\xi_B \left[\ln\frac{z}{\bar{x}}\, \frac{64 C_2 (\xi - \xi_B)^2 \exp\sqrt{4 N \ln z/\bar{x}(\xi - \xi_B)W_B^{-1}}}{3\sqrt{2\pi}\,\bar{x}/z}\, \frac{\exp\sqrt{4 N \ln z/\bar{x}(\xi - \xi_B)W_B}}{(16 N \ln z/\bar{x}(\xi - \xi_B)W_B^{-1})^{5/4}}\right]^2$$

$$\cdot\, \frac{1}{\sqrt{W_B}}\frac{4N}{4C_2}\frac{1}{2}\sqrt{\frac{4N \ln z/\bar{x}}{(\xi - \xi_B)W_B}}\cdot \exp\sqrt{N \ln z/\bar{x}\,\frac{\xi_B^2}{\xi - \xi_B}\, W_B^{-1}}\right\}.$$

With the same numbers as for the exclusive cross section and with $\xi_{max} = 0.3$ ($k^2_{\perp max} = 20\,\text{GeV}^2$) we find the same order of magnitude as for the exclusive cross section

$$0.01\text{--}0.1 \text{ events/day}. \tag{4.26}$$

Again we have to emphasize that this result takes into account only those parts of the Feynman diagrams which are most singular in the small-x region. Our numerical estimate indicates that at Hera energies nonleading terms are still quite important and, most likely, will lead to a decrease of the event rate (4.26).

The estimate (4.20) is in qualitative agreement with an earlier estimate [16] (with a branching ratio of $\approx 3\%$ for the μ-decay, (4.21) leads to a cross section $d\sigma \approx 10^{-37}\,\text{cm}^2$). What is new is the fact that the inclusive cross section does not significantly increase the event rate: the enhancement factor compared to the exclusive process is of the order 3–5 but certainly less than 10. When estimating the cross sections (4.15) and (4.25) one sees the interplay of two effects: a decrease as a function of the Z-mass, and an exponential increase if the scaling variables x and $\tilde{x}$ become small (as we have discussed before, the smallest allowed value for $\tilde{x}$ is determined through the incoming proton momentum as well as the Z-mass). At Hera energies the exponential factor is already quite large, and a further increase of the proton momentum by a factor 5 would already lead to a factor $\sim 10^2$ for the cross section!

V. Conclusions

In this paper we have extended the analysis of QCD planar ladder diagrams in the small-x region to the more general case where the momentum transfer r_μ along the ladder is different from zero, and where the full diagrams are evaluated as opposed to their energy discontinuity. As the main qualitative result we have found that r_μ has to be small in order to preserve the familiar small-x enhancement. A large transverse component $r_\perp$ prevents the formation of large powers of $\ln\ln Q^2$, whereas a large longitudinal component stops the growth at small x-values.

An immediate application is the study of certain exclusive and inclusive cross section which have not yet been studied in the framework of perturbative QCD. The exclusive cross section is obtained in a straightfor-

ward manner, whereas the inclusive cross section requires further analysis and leads to a formula which parallels the triple-Regge analysis of hadron-hadron scattering. As a practical example we have estimated the event rate for diffractive Z^0-photoproduction in ep-collisions: for the exclusive production we find an event rate of $1/3 - 1/2$ events/day ($\gtrsim 10^{-2}$ events/day in the $\mu^+\mu^-$-decay mode). The inclusive cross section gains only a factor < 10 over the exclusive case.

Strong motivation for studying the nonforward QCD ladders comes from interest in the $x \to 0$ behavior of the deep inelastic structure function. When $x \to 0$, it is believed that diagrams with the exchange of more than one QCD ladder become more and more important: this leads to a study of hyper-Feynman diagrams with QCD-ladders as building blocks. As a first step, one might try to "close" the diagrams of Fig. 8 at the upper end and integrate over the momentum r_μ along the ladders. Results of such an attempt will be presented in a future paper.

References

1. For a review see Refs. [2–6]
2. C.H.Llewellyn Smith: Schladming-Lectures 1978
3. Yu.L.Dokshitzer, D.I.Dyakonov, S.T.Troyan: Phys. Rep. **58**, 269 (1980)
4. E.Reya: Phys. Rep. **69**, 159 (1981)
5. A.H.Mueller: Phys. Rep. **73**, 237 (1981)
6. G.Altarelli: Preprint Univ. Rome 783 (1981) (to appear in Phys. Rep.)
7. L.V.Gribov, E.M.Levin, M.G.Ryskin: Phys. Lett. B **101**, 185 (1981)
8. T.Jaroszewicz, J.Kwiecinski: Orsay LPTHE 81/12
9. A.H.Mueller: Phys. Rev. D **18**, 3705 (1978)
10. G.P.Lepage, S.J.Brodsky: Phys. Rev. D **22**, 2157 (1980)
11. Yu.L.Dokshitzer: Sovj. Phys. JETP **46**, 641 (1977)
12. E.A.Kuraev, L.N.Lipatov, V.S.Fadin: Sovj. Phys. JETP **45**, 199 (1977)
13. S.-J.Chang, S.-K.Ma: Phys. Rev. **188**, 2385 (1969)
14. See [3] and K.Konishi, A.Ukawa, G.Veneziano: Nucl. Phys. B **157**, 45 (1979)
15. Particle Data Group, Rev. Mod. Phys.: 52 Part II, 1 (1980)
16. Study on the Proton-Electron Storage Ring Project Hera. EcFA 80/42 (1980). Desy Hera 80/01
17. S.Pakwasa, D.Prashar, S.F.Tuan: Phys. Rev. D **10**, 2124 (1974)
18. J.J.Sakurai: Erice-Lectures 1980